Computers and Fluids 149 (2017) 194–204

Contents lists available at ScienceDirect

Computers and Fluids

journal homepage: www.elsevier.com/locate/compfluid

Deviation analysis of loosely coupled quasi-static method for fluid-thermal interaction in hypersonic flows

Shaolong Guo [a], Yongliang Feng [a,b], Wen-Quan Tao [a,*]

[a] Key Laboratory of Thermo-fluid Science and Engineering of MOE, School of Energy & Power Engineering, Xi'an Jiaotong University, Xi'an 710049, China
[b] Institut Jean le Rond d'Alembert, UMR 7190, Université Pierre et Marie Curie-Paris 6, 4 place Jussieu-case 162, F-75252, France

ARTICLE INFO

Article history:
Received 21 October 2016
Revised 14 March 2017
Accepted 15 March 2017
Available online 24 March 2017

Keywords:
Hypersonic
Deviation
Formula
Loosely coupled method
Fluid-thermal interaction

ABSTRACT

Fluid-thermal interaction plays an important role in the design and development of hypersonic vehicles. Among the different ways to couple the flow field with the material thermal response, the loosely coupled quasi-static method is widely used. In this paper, deviation formulas based on one-dimensional model are derived for uncoupled method and loosely coupled quasi-static method to estimate the structural temperature deviations at the stagnation point in different forward time steps. To verify the formulas, fluid-thermal coupling numerical simulations are conducted for 2-D and 3-D hypersonic fluid-thermal interaction problems. The results show that the temperature deviation formulas agree quite well with the deviations from numerical simulation. The derived deviation formulas can serve as some guidance for selecting an appropriate forward time step for the loosely coupled quasi-static method.

1. Introduction

Due to the severe aerodynamic heating, thermal protection systems (TPS) for hypersonic vehicles are very important. In the design of the TPS, flow-thermal analysis methods are usually used to obtain an accurate and quick prediction of the structural temperatures. Traditionally, the prediction has been accomplished by using the uncoupled flow-thermal analysis method [1]. The recognized shortcoming of this approach is ignoring the effects of the boundary heat flux variation. Actual fluid-thermal interaction is a multi-field coupled physical problem. The difficulty of solving this problem is that physically the fluid and thermal structure have very different time scales. Usually, the characteristic time of the thermal response in the structure is much larger than that of the fluid flow process. Thus, the quite different time steps are required to accurately compute fluid and thermal responses. Currently, there are two partitioned ways to couple the flow field with the structure thermal response. One is the fully transient method, which advances the flow field and thermal structure response in real time at each time step [2]. The other is loosely coupled quasi-static method, which assumes that the hypersonic flow reaches a steady state in each forward time step. This assumption is based on the idea that the characteristic time of the fluid flow is several orders of magnitude smaller than that of the thermal structure response [3]. Therefore, the flow behavior approaches a steady state much more rapidly than the thermal response of the structure. Considering both computational cost and accuracy, the loosely coupled quasi-static approach is more widely adopted than the fully transient method.

In 1988, Thornton and Dechaumphai studied flow-thermal-structural interaction for aerodynamically heated panels (AHP) by using the loosely coupled method [1]. In the study, hypersonic flow was considered to be in quasi-static state. Since then different practices were adopted in literatures, only some typical works are mentioned here. Conti and Groener used the fully transient method to couple the flow field with the material response which involved ablation and shape change [4]. In the fully transient method, the flow field, material response and body shape were advanced in real time at each time step. Chen et al. implemented the loosely coupled quasi-static approach in the design of TPS of spacecraft [5]. For most of the trajectory points, the hypersonic flow was assumed in a quasi-static state and the flow solutions were obtained by using GIANTS codes. It is worth mentioning that this study [5] firstly indicated that the coupling method can be applied to the design of TPS of spacecraft. Yamamoto and Yoshioka coupled the CFD FVM solver with a thermal response FEM solver in a loosely coupled manner to obtain the material temperature of orbital reentry experiments (OREX) [6]. Hassan et al.

Abbreviations: AHP, aerodynamically heated panels; AUSMPW, advection upwind splitting method by pressure-based weight function; CFD, computational fluid dynamics; CSD, computational structural dynamics; CTD, computational thermodynamics; FEM, finite element method; OREX, orbital reentry experiments; TPS, thermal protection systems.

* Corresponding author.
E-mail address: wqtao@mail.xjtu.edu.cn (W.-Q. Tao).

http://dx.doi.org/10.1016/j.compfluid.2017.03.017
0045-7930/

Nomenclature

Latin symbols

a	acoustic speed, m/s
c	specific heat, J/(kg K)
e	total energy, J/kg
M	Mach number
p	pressure, Pa
q_x, q_y	x and y components of heat flux, W/m^2
Q	heat flux, W/m^2
T	temperature, K
u, v	x and y components of velocity, m/s
x, y	cartesian coordinates, m

Greek symbols

α	thermal diffusivity, m^2/s
γ	specific heat ratio
δ	thickness, m
Δt	time step of discrete equation, s
$\Delta\tau_s$	forward time step, s
ε	relative deviation of excess temperature
θ	excess temperature, K
λ	thermal conductivity, W m^{-1} K^{-1}
μ	dynamic viscosity, Pa s
ρ	density, kg/m^3
τ	time, s

Subscripts

f	fluid domain
s	solid domain
W	wall
∞	freestream
0	initial
$\tau/1$	uncoupled
τ/N	loosely coupled

Dimensionless numbers

Fo	Fourier number
Pr	Prandtl number

used the loosely coupled fluid/thermal method for predicting the ablation of hypersonic vehicles [7]. They coupled a fluid flow code and a thermal response code through mass and energy balances at a common interface. At a trajectory point, the fluid flow code was used to obtain a steady-state flow field solution. Löhner et al. studied the fluid-structure-thermal interaction problems by using a loosely coupled method through uniting CFD, Computational Structural Dynamics (CSD) and Computational Thermo-Dynamics (CTD) codes [8]. Kuntz et al. presented an iterative method which was obtained by coupling the CFD code with the structural thermal response code to predict the ablation of hypersonic vehicle [9]. At a trajectory point, the steady-state flow field solution was obtained using the SACCARA code. Tran and Farhat used an integrated fluid-structure-thermal solver to analyze the aerodynamic heating of wing section of the F-16 fighter plane [10]. Culler and McNamara adopted a two-way coupled method to analyze the fluid-thermal-structural coupling problem [11,12]. Crowell et al. coupled the aerodynamic CFD model and the heat transfer FEM model by using a loosely coupled partitioned scheme [13]. Ostoich et al. studied the coupled fluid-thermal response of spherical dome in a Mach 6.59 laminar boundary layer [14]. Zhang et al. used a loosely coupled method to couple the CFD solver with a thermo-structural dynamics FEM solver [15]. For each flight trajectory point, the steady-state CFD solver was used to get aerothermal loads.

Even though quite a few studies have been conducted on the uncoupled method and loosely coupled quasi-static method, there are few studies on the evaluation indicator to estimate the deviations caused by using the uncoupled method and loosely coupled quasi-static method. Practically, the accuracy estimation is very important and useful to determine an appropriate forward time step for obtaining predicted results with a specified deviation. As a first step in the study of this aspect, in this paper formulas will be derived for both uncoupled approach and loosely coupled quasi-static approach to estimate the deviations of structural temperatures at the stagnation point. To verify those formulas, coupled fluid-thermal problems are numerically studied on flow over a 2-D cylinder, a cone at Mach 6.47 and Mach 8 and a 3-D sphere at Mach 9.86. For the cases studied, the derived formulas for the estimation of deviation is quite successful. However, more research work is needed for applying this method to more complicated situations.

2. Governing equations

2.1. Governing equations for aerothermodynamics in the fluid domain

The compressible Navier–Stokes (N–S) equations for two-dimensional aerodynamic flow can be described as follows:

$$\frac{\partial \mathbf{U}}{\partial \tau}+\frac{\partial \mathbf{F}_1(\mathbf{U})}{\partial x}+\frac{\partial \mathbf{F}_2(\mathbf{U})}{\partial y}=\frac{\partial \mathbf{F}_{v1}(\mathbf{U})}{\partial x}+\frac{\partial \mathbf{F}_{v2}(\mathbf{U})}{\partial y} \tag{1}$$

where the vector $\mathbf{U}$ signifies the conservative variables. The vector in the present work is

$$\mathbf{U}=[\rho,\rho u,\rho v,\rho e]^T \tag{2}$$

Here, u and v are the x and y components of the velocity, respectively, and e is the energy per unit volume. The inviscid fluxes $\mathbf{F}_1$ and $\mathbf{F}_2$ are

$$\mathbf{F}_1(\mathbf{U})=\begin{pmatrix}\rho u\\ \rho u^2+p\\ \rho vu\\ u(\rho e+p)\end{pmatrix},\mathbf{F}_2(\mathbf{U})=\begin{pmatrix}\rho v\\ \rho uv\\ \rho v^2+p\\ v(\rho e+p)\end{pmatrix} \tag{3}$$

The corresponding viscous flux vectors are

$$\mathbf{F}_{v1}(\mathbf{U})=\begin{pmatrix}0\\ \sigma_{xx}\\ \sigma_{xy}\\ -q_x+u\sigma_{xx}+v\sigma_{xy}\end{pmatrix},\mathbf{F}_{v2}(\mathbf{U})=\begin{pmatrix}0\\ \sigma_{yx}\\ \sigma_{yy}\\ -q_y+u\sigma_{yx}+v\sigma_{yy}\end{pmatrix} \tag{4}$$

Here, q_x and q_y are the x and y components of the heat flux, respectively, and σ is the viscous stress tensor of the fluid. It is assumed that the fluid behaves like a calorically perfect gas. The pressure p can be calculated as follows:

$$p=(\gamma-1)\rho[e-(u^2+v^2)/2] \tag{5}$$

The dynamic viscosity of the air is determined by the following Sutherland formula.

$$\mu=1.458\times10^{-6}\frac{T^{3/2}}{T+110.4} \tag{6}$$

The thermal conductivity of the air can be calculated as $\lambda_f=c_p\mu/Pr$. For the air, the Prandtl number Pr is taken as 0.72.

2.2. Governing equations for structure thermal response

The structure thermal response is governed by the energy conservation equation which can be written in the following form:

$$\rho_s c_s\frac{\partial T}{\partial \tau}=\frac{\partial}{\partial x}\left(\lambda_s\frac{\partial T}{\partial x}\right)+\frac{\partial}{\partial y}\left(\lambda_s\frac{\partial T}{\partial y}\right) \tag{7}$$

where ρ_s is the material density, c_s is the material specific heat, λ_s is the material thermal conductivity.

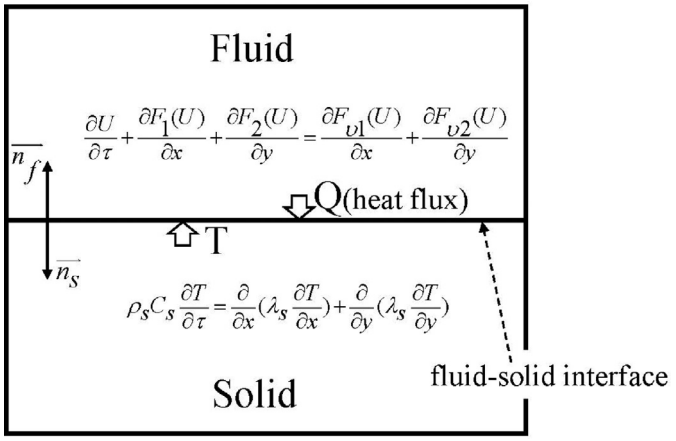

Fig. 1. Schematic of coupling relationship between the fluid and solid domains.

2.3. Interface coupling conditions

As illustrated in Fig. 1, the temperature and heat flux between the structure and fluid must be equal at the boundary, so the following conditions must be satisfied:

$$T_s = T_f \tag{8}$$

$$\lambda_s \nabla T_s \cdot \vec{n}_s = -\lambda_f \nabla T_f \cdot \vec{n}_f \tag{9}$$

Here, all of the variables are at the fluid-solid interface, T_s and ∇T_s are structure temperature and its gradient, T_f and ∇T_f are fluid temperature and its gradient, $\vec{n}_s$ and $\vec{n}_f$ are the unit normals of the structural and fluid boundaries.

3. Coupling procedure

3.1. Coupling analysis strategy

According to references [15–17], the coupled simulation can be divided into monolithic and partitioned approaches. In the monolithic approach, the equations are solved simultaneously. For the partitioned approach, the fluid and structure thermal response are calculated separately and coupled by exchanging the information at the interfaces in boundary condition treatments. This approach is adopted in this paper. Generally, different strategies used to determine the forward time steps of flow and structure thermal analysis give rise to different partitioned method.

As shown in Fig. 2, when conducting fluid-thermal interaction simulation, the structural wall temperature T_{W0} is imposed on the solid-fluid interface at the initial time, and the steady-state CFD solver is carried out to generate aerothermal load (wall heat flux Q_{W0}). The wall heat flux Q_{W0} is imposed on fluid-solid interface. For the uncoupled method, the transient thermal solver for the solid structure is used until the flight time ends, meaning that the heat flux Q_{W0} is kept unchanged during the entire simulation period. For the loosely coupled quasi-static method, the transient thermal solver is employed, for a time interval $\Delta\tau_s$ after which time the wall temperature rises to T_{W1}. The steady-state CFD solver is then carried out at the updated wall temperature to generate a new aerothermal load (wall heat flux Q_{W1}); This procedure is repeated until the flight time ends. The fully transient method is quite similar to the loosely coupled quasi-static method with following differences. One difference is that the heat flux is obtained by using an unsteady CFD solver, and the other is $\Delta\tau_s = \Delta\tau_f$ [2]. Among the three methods, the uncoupled one has the minimal computational cost but the worst accuracy, the fully transient method has the best accuracy but the maximum computational cost. The computational cost and accuracy of the loosely coupled quasi-static method are between these two methods. As an appropriate balance between computational cost and accuracy, the loosely coupled quasi-static method is widely used. The key is to select an appropriate forward time step such that both the accuracy and computational cost can be well balanced. In the following we will first analyze one-dimensional unsteady heat conduction problem to get the analytical expression for the excess temperature. Based on this results further discussion is conducted to finally obtain some guidance for selecting the appropriate forward time step.

3.2. Transient conduction analysis

As shown in Fig. 2, the thermal problem of the solid zone is a transient conduction issue with a given heat flux at the boundary. Usually, the structure is isothermal at the initial time without a heat source. The analytical transient heat conduction solution for the complicated practical structure is difficult to obtain. However, the transient heat conduction process in different geometries has very similar variation trends of their excess temperature, as it can be observed from the Heisler charts for three 1-D geometries (plate, cylinder and sphere) [18]. To simplify the analytical process, we will adopt a one-dimensional model with the same boundary condition to analyze the above-mentioned deviation. As illustrated in Fig. 3, for the one-dimensional model with the given boundary heat flux condition, the wall temperature at the left interface can be calculated using a Green function method as follows [19]:

$$T_W(\tau) = T_0 + \frac{1}{\rho_s c_s}\int_0^\tau Q_W(t) G(x=0, \tau\,|x'=0, t)\,\chi\, dt \tag{10}$$

where T_0 is the initial temperature, $Q_W(t)$ is the boundary heat flux, $G(x, \tau|x', t)$ is the Green function of this problem, and χ is the Sturm–Liouville weight function. For a flat plate, χ is equal to 1.

For a limited thickness flat plate as illustrated in Fig. 3, the one-dimensional transient conduction can be mathematically described as follows:

$$\begin{aligned}
&\frac{\partial T}{\partial \tau} = \alpha_s \frac{\partial^2 T}{\partial x^2}, 0 < x < \delta, \tau > 0\\
&BC1: -\lambda_s \frac{\partial T}{\partial x}|_{x=0} = Q_W(\tau)\\
&BC2: -\lambda_s \frac{\partial T}{\partial x}|_{x=\delta} = 0\\
&IC: T(x, \tau = 0) = T_0
\end{aligned} \tag{11}$$

For this problem, its Green function is [20]:

$$G(x, \tau|x', t) = \frac{1}{\delta} + \frac{2}{\delta}\sum_{m=1}^{\infty} \exp\left[-\frac{m^2\pi^2\alpha_s(\tau - t)}{\delta^2}\right] \times \cos\frac{m\pi x'}{\delta}\cos\frac{m\pi x}{\delta} \tag{12}$$

If the boundary heat flux is constant, the excess temperature at the left boundary can be obtained as follows:

$$\theta(\tau) = T(0, \tau) - T_0 = \frac{Q_W \delta}{\lambda_s}\left(Fo + \frac{2}{\pi^2}\sum_{m=1}^{\infty}\frac{1 - e^{-m^2\pi^2 Fo}}{m^2}\right) \tag{13}$$

where Fo is the Fourier number, defined by $Fo = \frac{\alpha_s \tau}{\delta^2}$. To simplify the expression, $G(x = 0, \tau|x' = 0, t)$ is abbreviated as $G(\tau; t)$. Following further analysis is based on the above 1-D model.

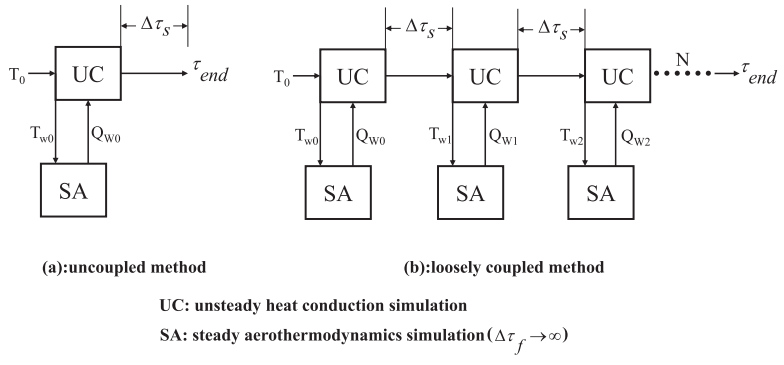

Fig. 2. The process of uncoupled and loosely coupled method.

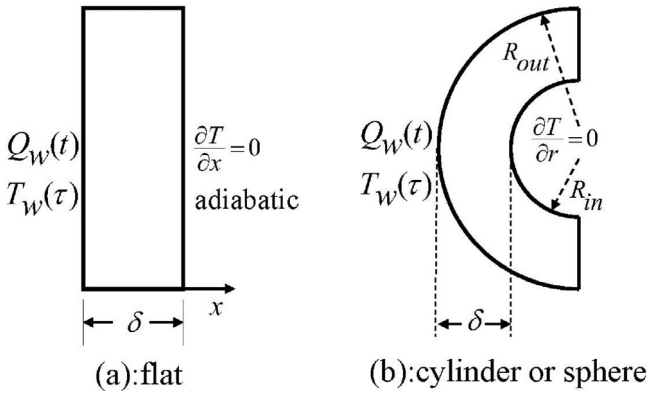

Fig. 3. One dimensional model of transient conduction.

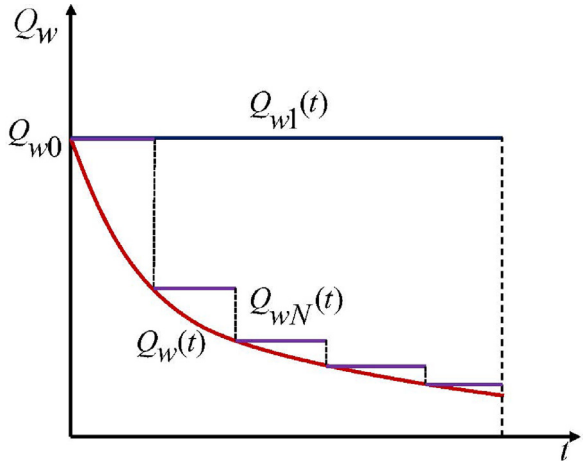

Fig. 4. Different boundary heat flux.

4. Relative deviation of excess temperature at the stagnation point

As shown in Fig. 4, $Q_W(t)$ represents the actual heat flux at the fluid-solid interface, and $Q_{WN}(t)$ is the heat flux at fluid-solid interface when using the loosely coupled quasi-static method. When using the uncoupled fluid-thermal analysis, the boundary heat flux is $Q_{W1}(t)=Q_{W0}$. Let $T_{W\tau 1}$ be the wall temperature at time τ for the uncoupled method. $Q_{W\tau 1}$ is the boundary heat flux obtained by using the steady-state CFD solver at the updated wall temperature $T_{W\tau 1}$.

4.1. Relative deviation of excess temperature for uncoupled method

According to the solution of one-dimensional transient conduction (Eq. (10)), relative deviation of excess temperature for the uncoupled approach at time τ can be described as follows:

$$\varepsilon_{\tau/1}=\frac{\theta_1(\tau)-\theta(\tau)}{\theta(\tau)}=\frac{\int_0^\tau[Q_{W0}-Q_W(t)]G(\tau;t)\chi\,dt}{\theta(\tau)\rho_s c_s} \tag{14}$$

where $\theta(t)$ is the actual excess temperature at the boundary and $\theta_1(t)$ is the excess temperature at the boundary when using uncoupled method. Usually, there is an approximate linear relationship between $Q_W(t)$ and $T_W(t)$ [21] at the stagnation point as follows:

$$Q_W(t)\approx A+BT_W(t) \tag{15}$$

Thus the relative deviation can be written:

$$\varepsilon_{\tau/1}=\frac{-\int_0^\tau B\theta(t)G(\tau;t)\chi\,dt}{\theta(\tau)\rho_s c_s} \tag{16}$$

By using the mean value theorem of integrals, the above equation can be written as:

$$\varepsilon_{\tau/1}=\frac{-\xi B\int_0^\tau G(\tau;t)\chi\,dt}{\rho_s c_s} \tag{17}$$

where the parameter ξ has the following mathematical expression:

$$\xi=\frac{\int_0^\tau\theta(t)G(\tau;t)dt}{\theta(\tau)\int_0^\tau G(\tau;t)dt} \tag{18}$$

For the uncoupled method, through Eqs. (10) and (15) one can obtain

$$\int_0^\tau G(\tau;t)\chi\,dt=\frac{\theta_1(\tau)\rho_s c_s}{Q_{W0}} \tag{19}$$

$$B=\frac{-Q_{W0}+Q_{W\tau 1}}{\theta_1(\tau)} \tag{20}$$

By substituting Eqs. (19) and (20) into Eq. (17), the relative deviation of the uncoupled method at the stagnation point can be written as follows:

$$\varepsilon_{\tau/1}=\xi\frac{Q_{W0}-Q_{W\tau 1}}{Q_{W0}} \tag{21}$$

Usually, Q_{W0} and $Q_{W\tau 1}$ can be obtained from numerical simulation when using the uncoupled method, and ξ can be calculated by Eq. (18).

If $\theta(t)$ is a monotonically increasing function, it can be obtained that $\xi\le 1$. Thus, the relative deviation has the following relationship.

$$\varepsilon_{\tau/1}\le\frac{Q_{W0}-Q_{W\tau 1}}{Q_{W0}}. \tag{22}$$

For the sustained hypersonic flight within the atmosphere, usually, the wall temperature function is a monotonically increasing one. Therefore, the above condition can be easily met.

For the exact expression of ξ of an arbitrary body, the actual excess temperature and Green function are required. Unfortunately, $\theta(t)$ is unknown and the expression of $G(\tau;t)$ can be very complex. Here, the one-dimensional model of a finite thickness flat plate as shown in Fig. 3 is used to calculate ξ. By substituting Eqs. (12) and (13) into Eq. (18), ξ can be obtained as follows:

$$\begin{aligned}\xi_{flat} &= \frac{\int_0^\tau \theta_{flat}(t)G_{flat}(\tau;t)dt}{\theta_{flat}(\tau)\int_0^\tau G_{flat}(\tau;t)dt} \\ &= \frac{\frac{\alpha_s\tau}{2\delta^2}+\frac{2\alpha_s}{\delta^2}\sum_{m=1}^{\infty}\int_0^\tau te^{-m^2\pi^2\frac{\alpha_s}{\delta^2}(\tau-t)}dt+\frac{2}{\pi^2}\sum_{n=1}^{\infty}\int_0^\tau\frac{1-e^{-n^2\pi^2\frac{\alpha_s}{\delta^2}t}}{n^2}dt}{\left[\frac{\alpha_s}{\delta^2}\tau+\frac{2}{\pi^2}\sum_{n=1}^{\infty}\frac{1-e^{-n^2\pi^2\frac{\alpha_s}{\delta^2}\tau}}{n^2}\right]\left[\tau+\frac{2\delta^2}{\alpha_s\pi^2}\sum_{m=1}^{\infty}\frac{1-e^{-m^2\pi^2\frac{\alpha_s}{\delta^2}\tau}}{m^2}\right]} \\ &+ \frac{\frac{4}{\pi^2}\sum_{n=1}^{\infty}\sum_{m=1}^{\infty}\int_0^\tau\frac{1-e^{-n^2\pi^2\frac{\alpha_s}{\delta^2}t}}{n^2}e^{-m^2\pi^2\frac{\alpha_s}{\delta^2}(\tau-t)}dt}{\left[\frac{\alpha_s}{\delta^2}\tau+\frac{2}{\pi^2}\sum_{n=1}^{\infty}\frac{1-e^{-n^2\pi^2\frac{\alpha_s}{\delta^2}\tau}}{n^2}\right]\left[\tau+\frac{2\delta^2}{\alpha_s\pi^2}\sum_{m=1}^{\infty}\frac{1-e^{-m^2\pi^2\frac{\alpha_s}{\delta^2}\tau}}{m^2}\right]}\end{aligned} \tag{23}$$

The convergence of the infinite series in Eq. (23) can be proved theoretically as follows. All the infinite series in the two terms of Eq. (23) are related with the following three types: $\sum_{n=1}^{\infty}\int_0^x\frac{1-e^{-n^2Ax}}{n^2}dx$, $\sum_{n=1}^{\infty}\int_0^x x'e^{-n^2A(x-x')}dx'$ and $\sum_{m=1}^{\infty}\sum_{n=1}^{\infty}\int_0^x\frac{e^{-m^2A(x-x')}}{n^2}dx'$. For the first type, it can be shown that $\sum_{n=1}^{\infty}\int_0^x\frac{1-e^{-n^2Ax'}}{n^2}dx'=\sum_{n=1}^{\infty}\frac{x}{n^2}+\frac{-1}{An^4}+\frac{e^{-n^2Ax}}{An^4}$, where A is a positive constant. While the second type has following relationship with the first one: $\sum_{n=1}^{\infty}\int_0^x x'e^{-n^2A(x-x)'}dx'=\frac{1}{A}\sum_{n=1}^{\infty}\int_0^x\frac{1-e^{-n^2Ax}}{n^2}dx'$. For the third type, $\sum_{m=1}^{\infty}\sum_{n=1}^{\infty}\int_0^x\frac{e^{-m^2A(x-x')}}{n^2}dx'=\sum_{m=1}^{\infty}\sum_{n=1}^{\infty}\frac{1-e^{-Am^2x}}{Am^2n^2}$.

From calculus it is known that for the infinite series $\sum_{n=1}^{\infty}a_n$, it is convergent if a_n equals to $\frac{1}{n}$, $\frac{1}{n^2}$ or $\frac{1}{n^4}$. Thus, the infinite series in Eq. (23) are convergent.

So, we can obtain the numerical solution of ξ_{flat}. By fitting the numerical solution of Eq. (23), the approximate function of ξ_{flat} can be obtained as follows:

$$\xi_{flat} \approx 0.706 - 0.208e^{-1.68/Fo} \tag{24}$$

In the above approximate function, the range of Fo is from 10^{-4} to 50. The value of R-square which is used to evaluate the fitting quality is 0.989. So, $\varepsilon_{\tau/1}$ of the uncoupled approach can be estimated as :

$$\varepsilon_{\tau/1} \approx (0.706 - 0.208e^{-1.68/Fo})\frac{Q_{W0}-Q_{W\tau 1}}{Q_{W0}} \tag{25}$$

4.2. Relative deviation of excess temperature for loosely coupled quasi-static method

When using the loosely coupled quasi-static fluid-thermal analysis, the boundary heat flux is $Q_{WN}(t)$. At time τ, the relative deviation of excess temperature for the loosely coupled quasi-static method can be described as follows:

$$\varepsilon_{\tau/N} = \frac{\theta_N(\tau)-\theta(\tau)}{\theta(\tau)} = \varepsilon_{\tau/1}(1-\beta) \tag{26}$$

where

$$\beta = \frac{\theta_1(\tau)-\theta_N(\tau)}{\theta_1(\tau)-\theta(\tau)} \tag{27}$$

According to Eq. (10), β can be calculated as follows:

$$\beta = \frac{\int_0^\tau[Q_{W0}-Q_{WN}(t)]G(\tau;t)\chi dt}{\int_0^\tau[Q_{W0}-Q_W(t)]G(\tau;t)\chi dt} \tag{28}$$

As illustrated in Fig. 4, it is assumed that the boundary heat flux $Q_{WN}(t)$ is a step-wise approximation along the curve of $Q_W(t)$. By substituting Eq. (15) into Eq. (28), β can be written as:

$$\begin{aligned}\beta &= \frac{\int_0^\tau[Q_{W0}-Q_{WN}(t)]G(\tau;t)\chi dt}{\int_0^\tau[Q_{W0}-Q_W(t)]G(\tau;t)\chi dt} \\ &= \frac{\sum_{i=1}^{N}[Q_{W0}-Q_{Wi}]\int_{\tau_{i-1}}^{\tau_i}G(\tau;t)\chi dt}{\int_0^\tau[A+BT_{W0}-A-BT_W(t)]G(\tau;t)\chi dt} \\ &= \frac{\sum_{i=1}^{N}-B\theta(\tau_{i-1})\int_{\tau_{i-1}}^{\tau_i}G(\tau;t)\chi dt}{\int_0^\tau -B\theta(t)G(\tau;t)\chi dt} = \frac{\sum_{i=1}^{N}\theta(\tau_{i-1})\int_{\tau_{i-1}}^{\tau_i}G(\tau;t)dt}{\int_0^\tau\theta(t)G(\tau;t)dt}\end{aligned} \tag{29}$$

where $N=\tau/\Delta\tau_s$

For the exact expression of β of an arbitrary body, the actual excess temperature and Green function are needed. Again, the one-dimensional model as described in Eq. (11) is approximately used to calculate β. By substituting Eqs. (12) and (13) into Eq. (29), it can be obtained that β is a function of Fo and N. The range of β value is given as follows:

$$1-\frac{1}{N} \le \beta \le 1 \tag{30}$$

So it can be obtained that:

$$\varepsilon_{\tau/N} \le \varepsilon_{\tau/1}/N \tag{31}$$

5. Numerical methodology

Numerical solutions for some typical geometries will be taken as references by which the above revised deviation formulas can be compared. In this section, the numerical methodology is presented for solving the fluid and structural thermal response problem, and in the next section numerical results will be presented. The governing equations for aerothermodynamics and structural thermal response are solved using the finite volume method. The transient term is advanced by using a third-order Runge–Kutta scheme [22]. The following time marching scheme is adopted.

$$\begin{aligned}U^{(1)} &= U^n + \Delta t R_h(U^n) \\ U^{(2)} &= \frac{3}{4}U^n + \frac{1}{4}U^{(1)} + \frac{1}{4}\Delta t R_h(U^{(1)}) \\ U^{(n+1)} &= \frac{1}{3}U^n + \frac{2}{3}U^{(2)} + \frac{2}{3}\Delta t R_h(U^{(2)})\end{aligned} \tag{32}$$

Here, the time step Δt which is used in the above equation to solve Eq. (1) or (7) is different from the forward time step $\Delta\tau_s$ (as shown in Fig. 2). The forward time step can be regarded as the time interval of exchanging the information at the interfaces.

For the N-S equations, AUSMPW+ scheme is used to discretize the convective flux, the viscous flux is computed using second-order central scheme. The AUSMPW+ scheme is an improvement of AUSMPW scheme. The purpose of the AUSMPW scheme is to combine the advantage of AUSM+ and AUSMD/V. In order to achieve this purpose, a pressure-based weight function is used. But the weight function is quite complicated. In the AUSMPW+, the weight function is simplified. The AUSMPW+ scheme has been used widely for the last fifteen years.

When using AUSMPW+ scheme, the numerical convective flux at the cell interface can be written as follows [23]:

$$\mathbf{F}_{1/2} = \bar{M}_L^+ a_{1/2}\mathbf{\Phi}_L + \bar{M}_R^- a_{1/2}\mathbf{\Phi}_R + (P_L^+\mathbf{P}_L + P_R^-\mathbf{P}_R) \tag{33}$$

(a) for $M_{1/2} \geq 0$

$$\begin{aligned} \bar{M}_L^+ &= M_L^+ + M_R^- \cdot [(1-w)(1+f_R) - f_L] \\ \bar{M}_R^- &= M_R^- \cdot w(1+f_R) \end{aligned} \tag{34}$$

(b) for $M_{1/2} < 0$

$$\begin{aligned} \bar{M}_L^+ &= M_L^+ \cdot w(1+f_L) \\ \bar{M}_R^- &= M_R^- + M_L^+ \cdot [(1-w)(1+f_L) - f_R] \end{aligned} \tag{35}$$

where

$$w(p_L, p_R) = 1 - \min\left(\frac{p_L}{p_R}, \frac{p_R}{p_L}\right)^3 \tag{36}$$

The details of $M^{\pm}$, $P_{L/R}^{\pm}$, $f_{L/R}$ can be found in [23]. In one dimension, $\mathbf{\Phi} = (\rho, \rho u, \rho H)^T$ and $\mathbf{P} = (0, p, 0)^T$.

The left and right states $\mathbf{\Phi}_L$, $\mathbf{\Phi}_R$ are obtained by using the third-order MUSCL scheme [23].

$$\begin{aligned} \mathbf{\Phi}_L &= \mathbf{\Phi}_i + \frac{1}{4}\left[\left(1-\frac{1}{3}\right)\overline{\nabla} + \left(1+\frac{1}{3}\right)\overline{\Delta}\right]_i \\ \mathbf{\Phi}_R &= \mathbf{\Phi}_{i+1} - \frac{1}{4}\left[\left(1-\frac{1}{3}\right)\overline{\nabla} + (1+\frac{1}{3})\overline{\Delta}\right]_{i+1} \\ \overline{\Delta}_i &= \text{minmod}[(\Phi_{i+1} - \Phi_i), \alpha(\Phi_i - \Phi_{i-1})] \\ \overline{\nabla}_i &= \text{minmod}[(\Phi_i - \Phi_{i-1}), \alpha(\Phi_{i+1} - \Phi_i)] \end{aligned} \tag{37}$$

$$\min \text{mod}(a, b) = sign(a)\max[0, \min(asign(b), bsign(a))],\ 1 \leq \alpha \leq 4 \tag{38}$$

For the structured body-fitted coordinate grids, Jacobi transformation is used to obtain the gradient of variable. The formulas can be written as follows [24]:

$$\frac{\partial \phi}{\partial x} = \frac{\partial \phi}{\partial \eta}\eta_x + \frac{\partial \phi}{\partial \kappa}\kappa_x \tag{39}$$

$$\frac{\partial \phi}{\partial y} = \frac{\partial \phi}{\partial \eta}\eta_y + \frac{\partial \phi}{\partial \kappa}\kappa_y \tag{40}$$

where η_x, η_y, κ_x, κ_y can be calculated by:

$$\eta_x = J^{-1}y_\kappa,\ \eta_y = -J^{-1}x_\kappa,\ \kappa_x = -J^{-1}y_\eta,\ \kappa_y = J^{-1}x_\eta \tag{41}$$

where J is the Jacobi factor, whose definition is:

$$J = x_\eta y_\kappa - x_\kappa y_\eta \tag{42}$$

For the unstructured grids, the gradient of variable is calculated using Gauss-Green reconstruction gradient method. For a control volume, the average gradient is calculated by the following expression [25]:

$$\nabla\phi = \frac{1}{\Delta V}\sum_{m=1}^{Num\_Face}\left(\phi \cdot \vec{S}\right)_m \tag{43}$$

where $(\phi \cdot \vec{S})_m$ is the product at the interface numbered by m. In this formula, the value of ϕ at the interface is calculated using arithmetic mean of two adjacent units.

6. Numerical results and discussion

To verify Eqs. (21) and (31), some 2-D and 3-D fluid-thermal coupling numerical simulations are studied. For the 2-D simulation, the hypersonic flows passing over a cylinder and a cone are considered. For each flow, two cases are calculated with Mach 6.47 and Mach 8, respectively. The structural thermal physical properties and initial free-stream conditions for Case 1 and Case 2 are given in Tables 1 and 2, respectively. For the 3-D simulation, the hypersonic flow passing over a sphere is studied. The simulation conditions are given in Table 3. In the comparison, the thermal responses calculated by the fully transient method are treated as the exact solution.

Table 1
The simulation conditions of Case 1.

Properties	Values
Solid density ρ_s, kg/m^3	8030
Solid specific heat capacity c_s, J/(kg K)	502.48
Solid thermal conductivity λ_s, W/(m K)	16.27
Initial free-stream T_∞, K	241.5
Initial free-stream Ma_∞	6.47
Initial free-stream P_∞, Pa	648.13

Table 2
The simulation conditions of Case 2.

Properties	Values
Solid density ρ_s, kg/m^3	7910
Solid specific heat capacity c_s, J/(kg K)	460
Solid thermal conductivity λ_s, W/(m K)	36.5
Initial free-stream T_∞, K	125.07
Initial free-stream Ma_∞	8.0
Initial free-stream P_∞, Pa	855.0

Table 3
The simulation conditions of Case 3.

Properties	Values
Solid density ρ_s, kg/m^3	8030
Solid specific heat capacity c_s, J/(kg K)	502.48
Solid thermal conductivity λ_s, W/(m K)	16.27
Initial free-stream T_∞, K	48.88
Initial free-stream Ma_∞	9.86
Initial free-stream P_∞, Pa	59.92

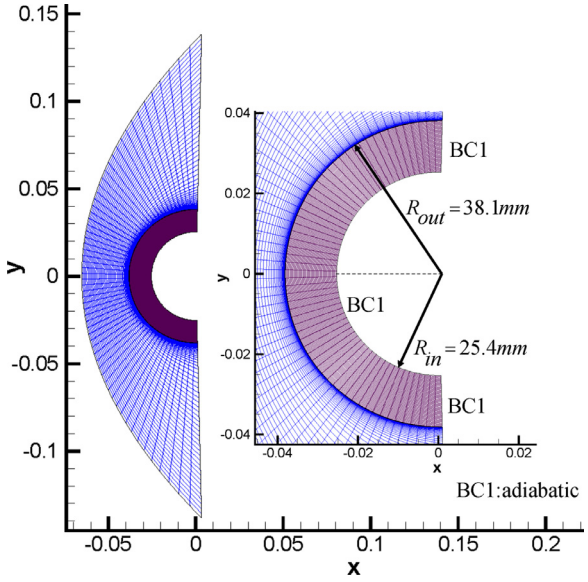

Fig. 5. Geometric dimensions and computational meshes.

6.1. The geometric shape and computational meshes

For the 2-D simulations, the two geometric shapes and the computational meshes used in the simulations are illustrated in Figs. 5 and 6, respectively. For the hollow cylinder shown in Fig. 5, the outer radius is 38.1 mm. The thickness of the cylinder wall is 12.7 mm. In the fluid domain, a structured grid system with 61×61 nodes is used in this simulation. In the boundary layer, clustered grid points are set for sufficient resolution. For the cone, as illustrated in Fig. 6, the total length is 50 mm. In the fluid domain, a structured mesh with 61×101 nodes is used. In the solid

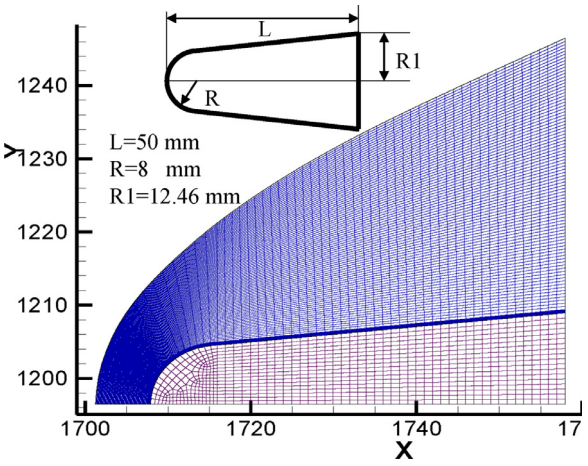

Fig. 6. Geometric dimensions and computational meshes.

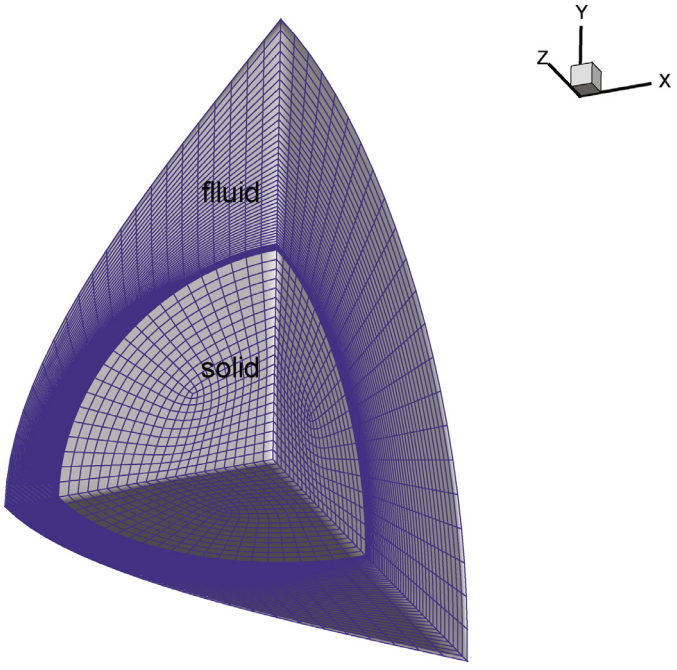

Fig. 7. Geometric dimensions and computational meshes.

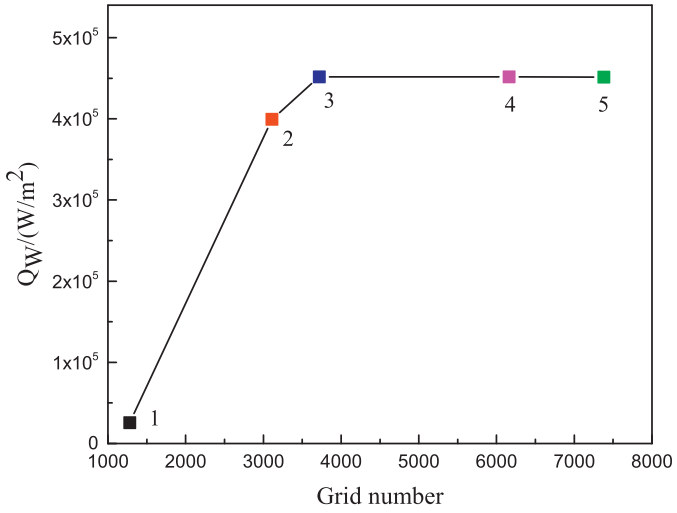

Fig. 8. Grid independence test in fluid domain.

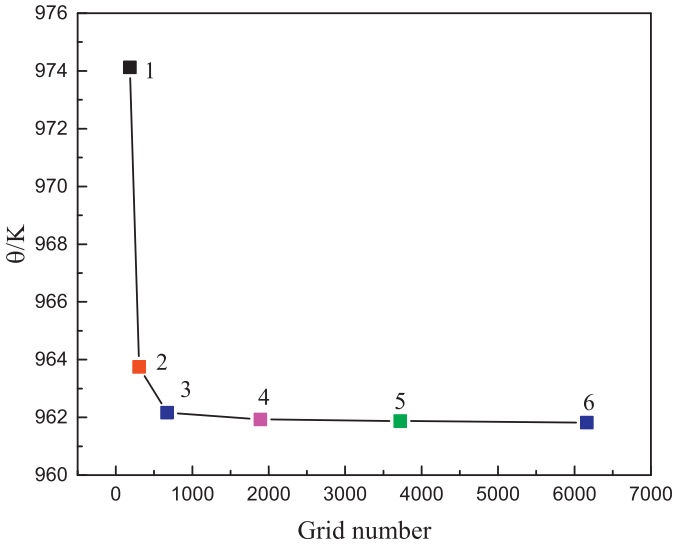

Fig. 9. Grid independence test in solid domain.

domain, an unstructured mesh is used. In those simulations, the initial structure temperature is 294.4 K.

For the 3-D simulations, the geometric shape and computational mesh are shown in Fig. 7. The radius of the sphere is 38.1 mm. In the fluid domain, 21,780 grid cells are used. In the solid domain, the initial temperature is 300 K.

The above meshes have been examined by grid independence tests. Taking the 2-D cylinder simulation for example, the grid independence tests under the Case 1 simulation condition for the fluid and solid regions are shown in Figs. 8 and 9, respectively. In the test simulations for fluid, the wall temperature is set to 294.4 K. Q_{W0} is the wall heat flux at the stagnation point when the hypersonic flow reaches a steady state. The difference in Q_{W0} among the third mesh which is used in the following fluid simulation and the last one is about 0.1%. So, the third mesh can be regarded as one that can provide grid independent solutions. In the test simulations for the solid, the wall heat fluxes obtained from the above simulation are set to the left boundary. θ is the excess temperature at the left boundary when $\tau_s = 100$ s. The difference in θ between the last two meshes is about 0.006%. So, the fifth mesh is used in the following solid simulation.

Initially, the structures are in uniform isothermal condition. Next, the hypersonic flow reaches a steady state under the initial and boundary conditions. The distributions of temperature and Mach number within the flow field of Case 1 of flow over the cylinder are illustrated in Fig. 10 as an example. After that, the fluid-thermal coupling numerical simulations are carried out. Taking the 3-D simulation for example, the temperature field on the solid domain obtained by using the fully transient method at time 81.9 s is shown in Fig. 11. For the other situations, similar distributions are obtained. For the simplicity of presentation, they are not shown here. We will focus on the accuracy analysis of the derived deviation prediction equations

6.2. Relative deviation of the uncoupled approach at the stagnation point

The uncoupled method is used to calculate the wall temperatures for different flight times (τ_{end}). The relative deviations of excess temperature at the stagnation point then can be obtained by comparing the uncoupled results with the fully transient method.

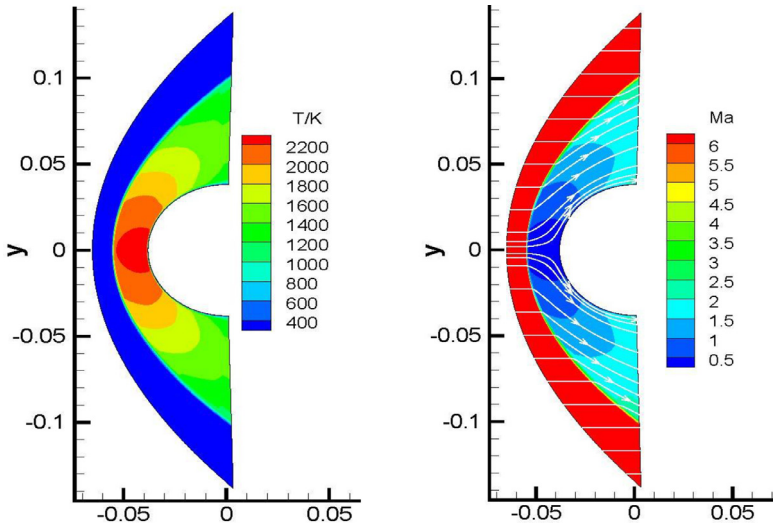

Fig. 10. Temperature and Mach distributions within the fluid.

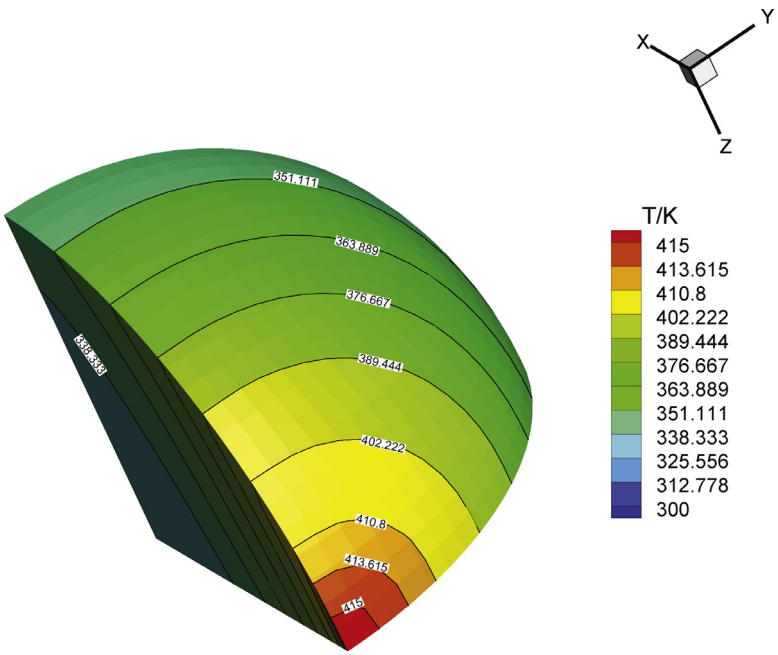

Fig. 11. Temperature distributions of the sphere.

For the cylinder, the deviations resulting from numerical simulation and from the formula for Case 1 and Case 2 are illustrated in Figs. 12 and 13, respectively. For the cone, they are illustrated in Figs. 14 and 15, respectively. The results of the sphere are shown in Fig. 16. In those figures, the black line represents the relative deviation between the uncoupled simulation and fully transient simulation. The relative deviation of uncoupled method in Eq. (21) is shown by the red line for the flat case.

From those figures, it can be seen that all the deviations obtained by numerical simulation are lower than those obtained from theoretical formula of one-dimensional model in which ξ is equal to 1. This fact coincides with the previous theoretical analysis.

Those figures show that the results predicted by the formula in which $\xi = \xi_{flat}$ agree well with the numerical simulation. As shown in Tables 1–3, Case 1, Case 2 and Case 3 have different structural thermal physical properties and initial free-stream conditions. It can be found that the theoretical formulas derived by adopting flat plate model ($\xi = \xi_{flat}$) can adapt to the structural thermal properties and flow conditions studied. In addition, it may be noted that from Figs. 12 to 16, appreciable deviation between $\xi = \xi_{flat}$ and $\xi = 1$ can be observed. This implies that for the flat case $\theta(t)$ is actually a monotonically increasing function of t, thus replacing the instant value of $\theta(t)$ by its maximum value $\theta(\tau)$ must lead to great differences. It is also interesting to point out that from these figures it can be seen that the deviation of the cone is greater compared with the cylinder. This is caused by different geometries between the cone and cylinder. The radius of the cone is 8 mm (Fig. 6), which is smaller than the radius of the cylinder (38.1 mm, Fig. 5). Usually, at the same initial free-stream conditions, the smaller the radius, the bigger the wall heat flux at the stagnation point. So the different boundary heat fluxes at the stagnation points lead to different deviations.

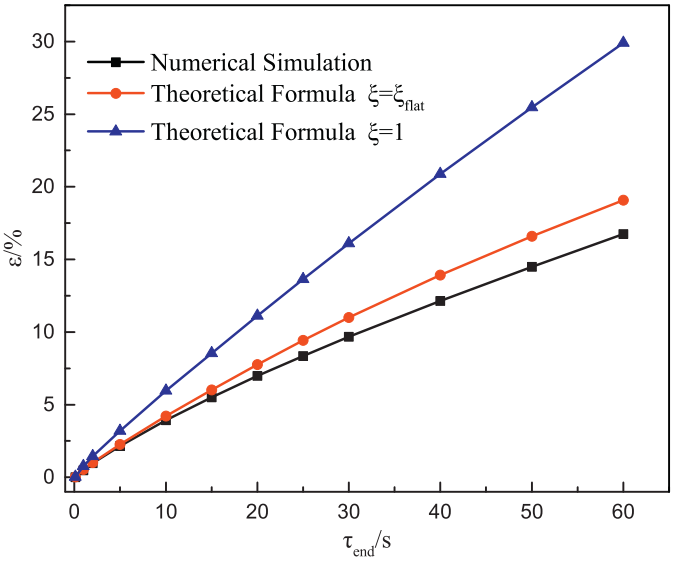

Fig. 12. Relative deviation of Case 1 of the cylinder.

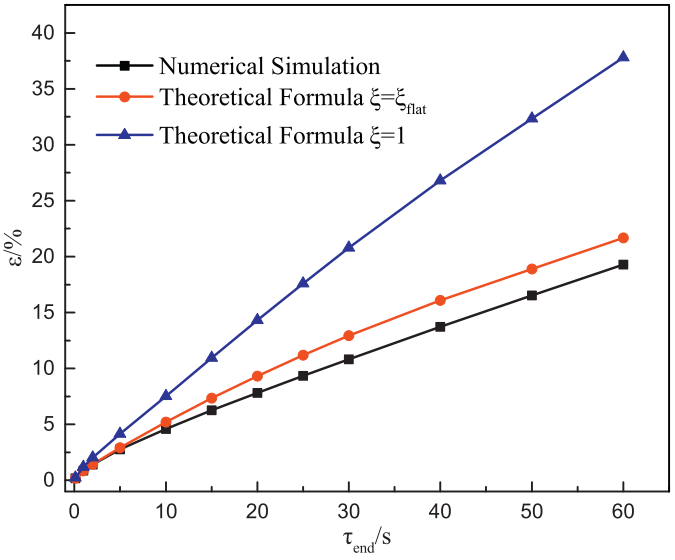

Fig. 13. Relative deviation of Case 2 of the cylinder.

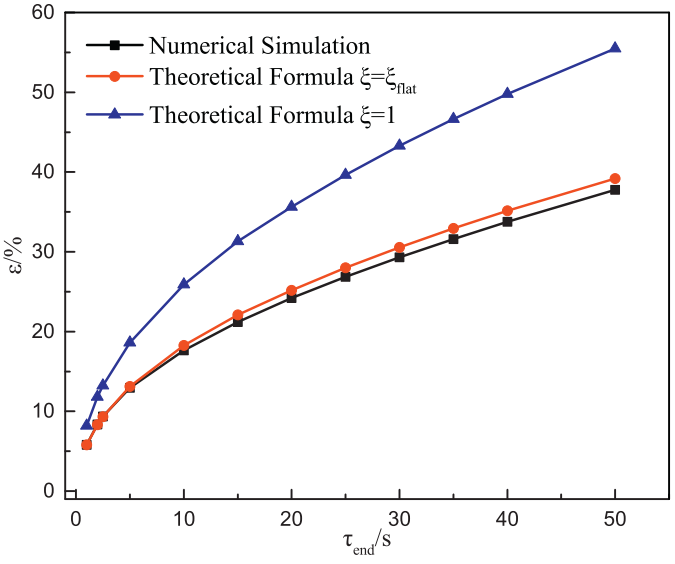

Fig. 14. Relative deviation of Case 1 of the cone.

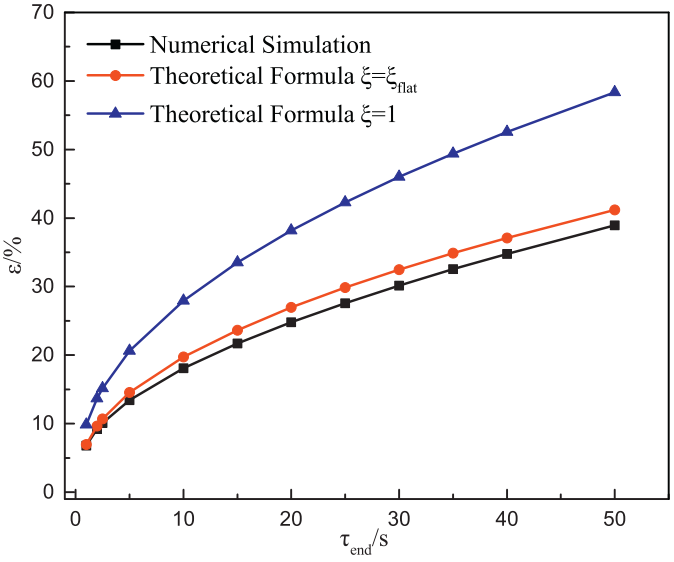

Fig. 15. Relative deviation of Case 2 of the cone.

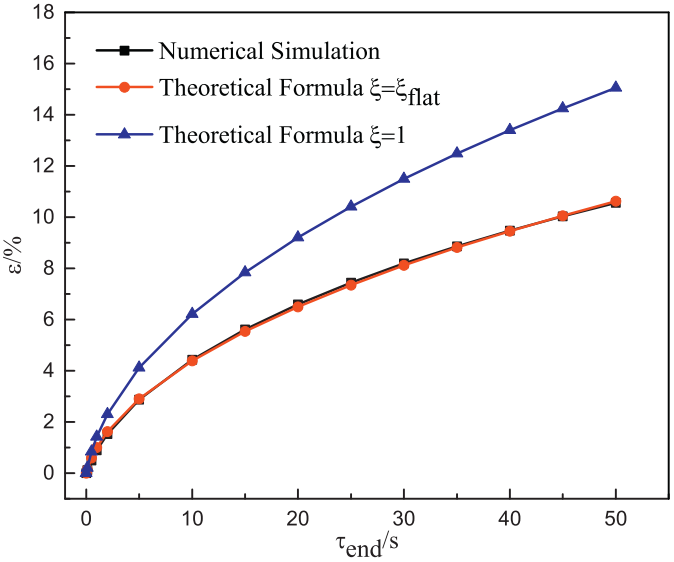

Fig. 16. Relative deviation of Case 3 of the sphere.

6.3. Relative deviation of loosely coupled quasi-static method at the stagnation point

The loosely coupled quasi-static method is used for different forward time steps ($\Delta\tau_s$). At flight time $\tau_{end} = 50$ s, the temperatures are compared with the fully transient method. For the cylinder, the relative deviation obtained by numerical simulation and the formula for Case 1 and Case 2 are illustrated in Figs. 17 and 18, respectively. For the cone, the relative deviation obtained by numerical simulation and the formula for Case 1 and Case 2 are illustrated in Figs. 19 and 20, respectively. The results of the sphere are shown in Fig. 21. In these figures, $N = \frac{50s}{\Delta\tau_s}$. It can be seen that the results of numerical simulation are less than $\frac{\varepsilon_{50s/1}}{N}$, which is in quite good agreement with the theoretical analysis.

When using the loosely coupled quasi-static method, usually there is no criterion to determine how large the values of forward time steps $\Delta\tau_s$ should be. Often it was determined by a trial and error practice. However, the values of $\Delta\tau_s$ are quite important. Usually, the bigger the value of $\Delta\tau_s$, the worse the simulation precision and the less the computational cost. When $\Delta\tau_s = \tau_{end}$, the

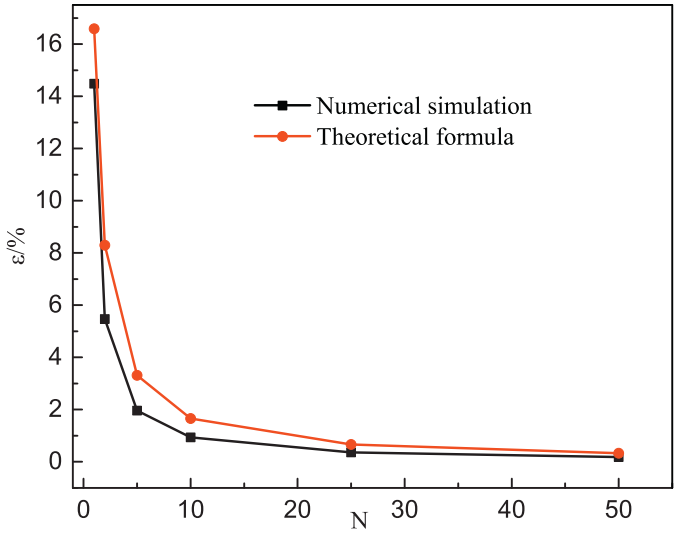

Fig. 17. Relative deviation of Case 1 of the cylinder.

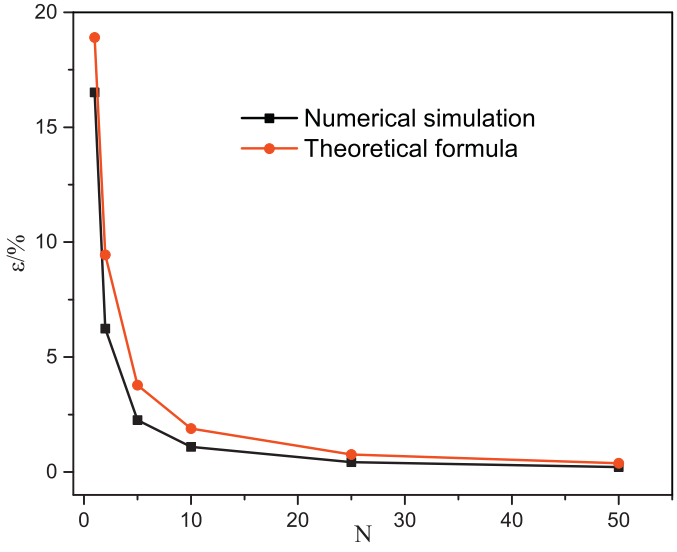

Fig. 18. Relative deviation of Case 2 of the cylinder.

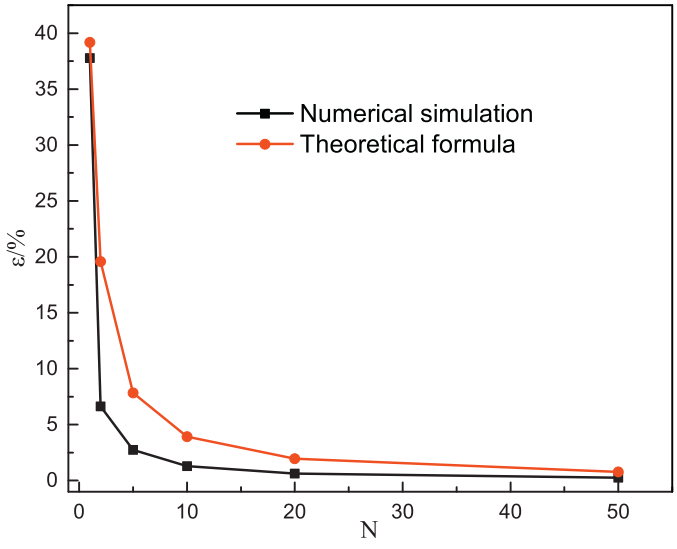

Fig. 19. Relative deviation of Case 1 of the cone.

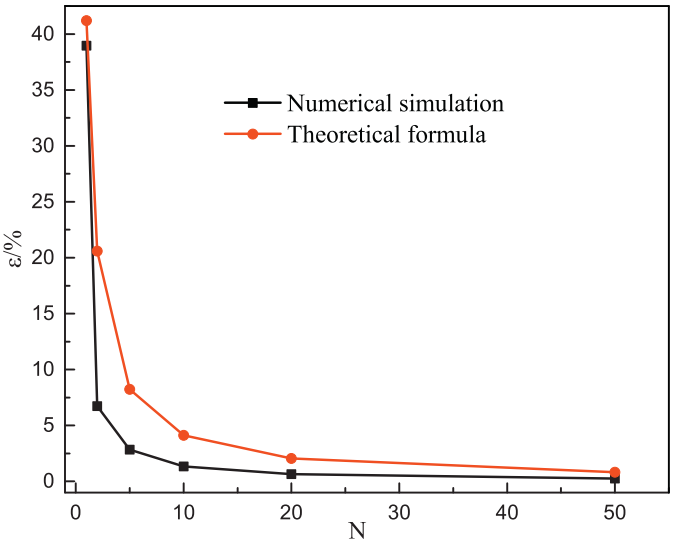

Fig. 20. Relative deviation of Case 2 of the cone.

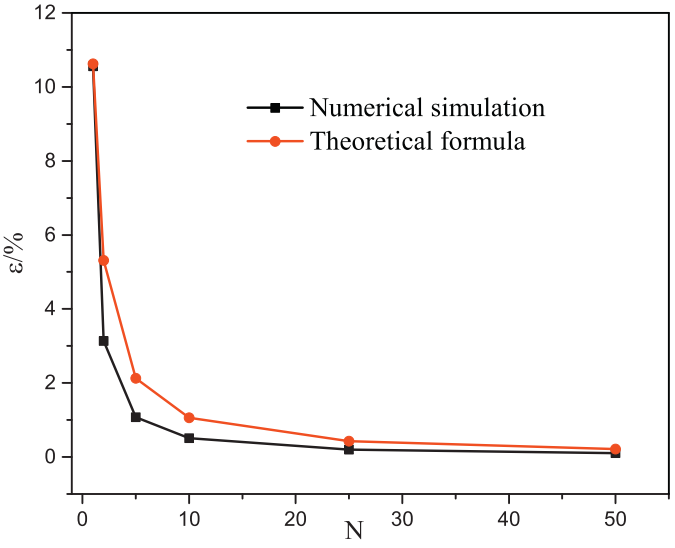

Fig. 21. Relative deviation of the sphere.

loosely coupled quasi-static method is equivalent to the uncoupled method which has the minimal computational cost but worst accuracy. From the above results, it can be seen that the relative deviation of the loosely coupled quasi-static method reduced rapidly when N is small, then with the increase of N, the relative deviation reduces very slowly. In the large N region, there is tremendous computational cost to obtain a small increase in accuracy. Figs. 17–21 therefore provide some guidance for selecting an appropriate forward time step in order to make a good balance between computational cost and accuracy.

7. Conclusion

Through analyzing the features of unsteady heat conduction of a one-dimensional model, theoretical formulas are derived to estimate the structural temperature deviations at the stagnation point for the uncoupled and loosely coupled quasi-static fluid-thermal methods. The fluid-thermal coupling numerical simulation is carried out to verify the present estimation formulas on hypersonic flow over a 2-D cylinder, cone and a 3-D sphere. For the uncoupled method, the results of the simulation agree well with the formula

in which $\xi = \xi_{flat}$. For the loosely coupled quasi-static method, the deviation of the numerical simulations are less than $\varepsilon_{\tau/1}/N$ which is consistent with the theoretical analysis. The derived deviation estimation formulas provide some guidance to select an appropriate forward time step for the loosely coupled quasi-static method with a specified prediction error.

Lastly, additional research is required before it is recommended that one implement this estimation method to significantly more complex problems. For example, when analyzing a complete hypersonic vehicle, the effects of the complex vehicle shape and the fluid-flow boundary conditions which vary with the transient trajectories on the estimation formulas should be studied.

Acknowledgments

This study is supported by the Key Project of International Joint Research of National Natural Science Foundation of China (51320105004) and 111 Project (B16038).

References

[1] Thornton EA, Dechaumphai P. Coupled flow, thermal, and structural analysis of aerodynamically heated panels. J Aircraft 1988;25(11):1052–9.
[2] Xia G, Liu XJ, Chen WK, Qin ZZ. Numerical simulation of coupled aero-heating and solid heat penetration for a hypersonic blunt body. J Natl Univ Def Technol 2003;25(1):35–9.
[3] Miller, BA, Crowell, AR, McNamara, JJ, Modeling and analysis of shock impingements on thermo-mechanically compliant surface panels, AIAA Paper 2012-1548.
[4] Conti, RJ, Groener, LS, Practical Navier-Stokes computation of axisymmetric reentry flowfields with coupled ablation and shape change, AIAA Paper 92-0752.
[5] Chen Y-K, Henline W, Tauber M. Mars pathfinder trajectory based heating and ablation calculations. J Spacecr Rockets 1995;32(2):225–30.
[6] Yamamoto, Y, Yoshioka, M, Cfd and fem coupling analysis of orex aerothermodynamic flight data, AIAA Paper 95-2087.
[7] Hassan, B, Kuntz, DW, Potter, DL, Coupled fluid/thermal prediction of ablating hypersonic vehicles, AIAA Paper 1998-168.
[8] Löhner R, Yang C, Cebral J, Baum JD, Luo H, Pelessone D, et al. Fluid-structure-thermal interaction using a loose coupling algorithm and adaptive unstructured grids 29th AIAA fluid dynamics conference; 1998.
[9] Kuntz DW, Hassan B, Potter DL. Predictions of ablating hypersonic vehicles using an iterative coupled fluid/thermal approach. J Thermophys Heat Transf 2001;15(2):129–39.
[10] Tran, H, Farhat, C, An integrated platform for the simulation of fluid-structure-thermal interaction problems, AIAA Paper 2002-1307.
[11] Culler AJ, McNamara JJ. Studies on fluid-thermal-structural coupling for aerothermoelasticity in hypersonic flow. AIAA J 2010;48(8):1721–38.
[12] Culler AJ, McNamara JJ. Impact of fluid-thermal-structural coupling on response prediction of hypersonic skin panels. AIAA J 2011;49(11):2393–406.
[13] Crowell AR, Miller BA, McNamara JJ. Computational modeling for conjugate heat transfer of shock-surface interactions on compliant skin panels. In: 13th AIAA dynamics specialists conference; 2011. p. 1–18.
[14] Ostoich CM, Bodony DJ, Geubelle PH. Fluid-thermal response of spherical dome under a Mach 6.59 laminar boundary layer. AIAA J 2012;50(12):2791–808.
[15] Zhang, ST, Chen, F, Liu, H, Integrated fluid-thermal-structural analysis for predicting aerothermal environment of hypersonic vehicles, AIAA Paper 2014-1394.
[16] Kazemi-Kamyab V, van Zuijlen AH, Bijl H. A high order time-accurate loosely-coupled solution algorithm for unsteady conjugate heat transfer problems. Comput Methods Appl Mech Eng 2013;264:205–17.
[17] Zhao XL, Sun ZX, Tang LS, Zheng GT. Coupled flow-thermal-structural analysis of hypersonic aerodynamically heated cylindrical leading edge. Eng Appl Comput Fluid Mech 2011;2(5):170–9.
[18] Cengel YA, Ghajar AJ. Heat and mass transfer: fundamentals and applications. New York: McGraw-Hill; 2011. p. 240–2.
[19] Hahn DW, Ozisik MN. Heat conduction. Hoboken, America: John Wiley & Sons; 2012.
[20] Jia L, Fang ZH, Qian XH. Advanced heat transfer. Beijing, China: Higher Education Press; 2003.
[21] Huang T, Mao GL, Jiang GQ, Zhou W. Two dimensional coupled flow-thermal-structural numerical simulation. Acta Aerodyn Sinica 2000;18(1):115–19.
[22] Fu DX, Ma YW, Li XL, Wang Q. Direct numerical simulation of compressible turbulent flow. Beijing, China: Science Press; 2010.
[23] Kim KH, Kim C, Rho O-H. Methods for the accurate computations of hypersonic flows: I. ausmpw+ scheme. J Comput Phys 2001;174(1):38–80.
[24] Tao WQ. Numerical heat transfer. Xian, China: Xian Jiaotong University Press; 2001.
[25] Tao WQ. Recent advances in computational heat transfer. Beijing, China: Science Press; 2005.